

# Chiral quark model study of the $NN$ system within a Lippmann-Schwinger resonating group method

D. R. Entem, F. Fernández, and A. Valcarce

*Grupo de Física Nuclear, Universidad de Salamanca, E-37008 Salamanca, Spain*

(Received 22 March 2000; published 7 August 2000)

We analyze the two-nucleon system below the pion threshold, using a chiral quark cluster model. We solve multichannel resonating group method equations in momentum space, treating them as a set of Lippmann-Schwinger equations. Deuteron data and scattering phase shifts up to a total angular momentum  $J=6$  are presented. Full couplings to  $N\Delta$  and  $\Delta\Delta$  channels are considered and analyzed. High angular momentum partial waves ( $L>2$ ) provide a detailed test of chiral symmetry in the two-nucleon system.  $D$  waves still show important short-range effects. Low angular momentum partial waves and deuteron observables are in good agreement with the experimental data, showing that the underlying quark structure provides the required short-range potential behavior.

PACS number(s): 13.75.Cs, 12.39.Jh, 24.85.+p

## I. INTRODUCTION

The understanding of the interaction between two nucleons remains a fundamental problem in nuclear physics. There is no doubt that explicit quark degrees of freedom are required in order to describe deep-inelastic scattering at high momentum transfer; however, it is still unclear how the nuclear forces arise from the fundamental quark interactions. This difficulty is due to the non-Abelian character of QCD, which implies that the gauge bosons (gluons) carry a color charge and can couple to one another. On one hand, these nonlinear couplings lead to asymptotic freedom which allows to carry out meaningful perturbative calculations at high energies. On the other hand, the quark-quark force becomes extremely strong in the low-energy regime (the realm of nuclear physics), and this makes the calculations very hard and has prevented thus far any direct solution of the QCD equations. For this reason, the most accurate descriptions of the  $NN$  scattering data and deuteron properties have been done in terms of multiboson exchanges at the baryon level, in the framework of old-fashioned perturbation theory (i.e., the Bonn potential [1]). Although the agreement with experiment is impressively good, the justification of such approaches in terms of QCD remains unclear.

During the last decade, there has been an effort to understand the  $NN$  force in a more fundamental way, based on the symmetries of QCD. Although we are largely ignorant of the nonperturbative dynamics of QCD at low energies, we know that an approximate chiral symmetry exists, which is broken by the vacuum. The spontaneous breakdown of a symmetry translates into the appearance of massless modes, the Goldstone bosons. However, since chiral symmetry is only approximate, we expect the associated Goldstone boson (i.e., the pion) to have a small but finite mass. As a consequence, QCD could be described in terms of an effective chiral Lagrangian (with the Goldstone pions and the nucleons as the relevant degrees of freedom), similar to the effective chiral Lagrangian for nuclear forces proposed by Weinberg [2].

A low-energy chiral Lagrangian of this type, providing a nonlinear realization of the  $SU(2)_L \times SU(2)_R$  chiral symmetry, has been used by Ordoñez, Ray, and van Kolck [3] for

the two-nucleon problem. These authors calculate the one and two-pion  $NN$  potential, and use more than 20 parameters to generate the short-range potential by means of contact terms. A good fit is obtained for the deuteron and for low partial waves below the pion threshold, but the large number of parameters obscures the role of chiral symmetry in the  $NN$  interaction. Recently, Epelbaum, Glöckle, and Meissner [4] have been able to reproduce the deuteron properties and  $NN$  phase shifts by means of a chiral nucleon-nucleon potential, including one and two-pion exchanges (up to the next-to-next-to-leading order) and contact interactions parametrized in terms of only nine parameters.

A possible way of avoiding the introduction of a large number of parameters in these models is that of abandoning a complete description of the  $NN$  observables, and exploring only those regions which are governed by chiral symmetry alone. This approach has been pursued by Kaiser, Brockmann, and Weise [5], who calculate  $NN$  phase shifts with orbital angular momentum  $L \geq 2$  using an effective chiral Lagrangian and a minimal set of parameters. An alternative way is provided by the chiral quark cluster model (CQC) [6]. The starting point of this approach is the realization that, at low energies, the relevant degrees of freedom are not the current quarks of the QCD Lagrangian, but, rather, the constituent quarks. Constituent quark mass and chiral symmetry are closely related concepts. If one assumes that the chiral symmetry is spontaneously broken at an energy scale higher than the confinement scale, quarks acquire the constituent masses at energies in between these two scales. Then, baryons are described as clusters of three confined constituent quarks, interacting through gluons and through the elementary Goldstone bosons of the spontaneously broken symmetry. Minimal chiral symmetry is realized by means of two fields corresponding to the exchange of a pseudoscalar and a scalar Goldstone boson.

This model not only reduces the number of parameters, but also has several advantages concerning the description of the baryon-baryon potential. Chiefly, by keeping the fundamental interactions at the quark level, it is possible to take full advantage of the quark antisymmetry, which provides a mechanism to generate the short-range  $NN$  repulsion [7]. This is an important difference with respect to those potentials where the short-range part is produced by fitting contact

terms. Quark antisymmetry allows us to predict the short-range behavior of less known systems (like  $N-\Delta$  or  $\Delta-\Delta$ ) in a completely parameter-free way. By contrast, the fitted short-range  $NN$  potentials do not permit such immediate generalizations. Besides, the use of quark antisymmetry provides a method for treating the nucleon and its resonances  $\Delta$ ,  $N^*$ ,  $\dots$ , in a single framework, without having to increase the number of parameters. Finally, this approach opens the door to a consistent description of the baryon structure and of the baryon-baryon interaction.

Based on the liquid instanton model, Fernández *et al.* [6] derived a quark-quark interaction in the QCD scheme, which has been applied to the description of the  $NN$  scattering phase shifts and to the study of static and electromagnetic properties of the deuteron. The calculations were done using the resonating group method (RGM) in configuration space below the pion threshold, and including the coupling of the  ${}^5D_0^{N\Delta}$  channel to the  ${}^1S_0^{NN}$  partial wave. This tensor coupling is very similar to the  ${}^3D_1^{NN}-{}^3S_1^{NN}$  in the deuteron case, and generates the additional attraction needed to reproduce the experimental data [8].

With this paper, we undertake a description of the two-nucleon problem in momentum space below and above the pion threshold, based on the CQC model. If one wants to go above pion threshold, then it is more convenient to work in momentum space, for several reasons. First of all, the calculation in coordinate space (which gives accurate results up to 300 MeV of laboratory energy) is hardly applied at higher energies, due to the rapid oscillation of the relative wave function. Besides, the multichannel calculations including nucleon resonances are quite naturally done in momentum space, due to the parametrization of the resonance widths.

In the present work, we will formulate the momentum space RGM calculation, introducing an alternative method for the solution of the coupled RGM equations, here treated as a set of coupled Lippmann-Schwinger equations. After a detailed description of the technical aspects, the method will be tested by studying scattering and bound-state problems of the  $NN$  system below the pion threshold. We will pay special attention to high angular momentum partial waves ( $L \geq 3$ ), never studied within the model. The deuteron and low angular momentum partial waves ( $L \leq 2$ ) are also studied, emphasizing the effect of the full coupling to  $N\Delta$  and  $\Delta\Delta$  channels. In a future work, we plan to extend our calculations to above the pion threshold.

The paper is organized as follows. In the next section, we review the main aspects of the chiral quark cluster model. Section III is devoted to the formulation of RGM in momentum space and to its numerical solution. An estimate of the model parameter values is given in Sec. IV. In Sec. V, we study the two-nucleon bound-state problem, i.e., the deuteron. A detailed analysis of the influence of  $\Delta\Delta$  channels in the deuteron properties is performed. Section VI is dedicated to the study of the  $NN$  phase shifts for low and high angular momentum partial waves. Finally, in Sec. VII we provide a summary of the main results of our work.

## II. THE CHIRAL QUARK CLUSTER MODEL

The QCD Lagrangian with massless quarks for  $N_f$  flavors possesses a global symmetry under  $SU(N_f) \times SU(N_f)$  inde-

pendent rotations of the left and right-handed quark fields: the chiral symmetry. If this symmetry were exact, one would observe chiral multiplets similar to those relating to the almost exact invariance of strong interactions under isospin rotations (e.g., the doublet  $p-n$  and the triplet  $\pi^+ - \pi^0 - \pi^-$ ). However, splittings between chiral partners are huge. For example, the splitting between the vector  $\rho$  and the axial  $a_1$  mesons is about 500 MeV (2/3 of the  $\rho$  mass) and the splitting between the nucleon and its chiral partner is even larger (939–1535). These splittings are indeed too large to be explained by the small current quark masses, which break chiral symmetry from the very beginning. The only conclusion one can draw from these data is that the chiral symmetry of QCD is spontaneously broken starting at a certain scale  $\Lambda_{\chi SB}$ .

Some years ago, Shuryak [9] proposed a QCD vacuum model that explains in a simple and elegant way the spontaneous breaking of chiral symmetry. This model, developed later on by Diakonov *et al.* [10], suggests that the QCD partition function is dominated by fluctuations of the gluonic field of instanton type, with quantum oscillations around it. In this sense, the QCD vacuum is seen as an instanton liquid, plus small quantum fluctuations of the gluonic field. This suggestion was recently tested by calculations on the lattice, showing that a decrease of the gluonic field fluctuations (called a *cooling* process) leaves as the only surviving configurations those of instanton and anti-instanton type [11].

When light quarks are put into the instanton vacuum, they develop a momentum-dependent dynamical mass which can be identified with the constituent mass. This dynamical mass breaks the chiral symmetry and, according to the Goldstone theorem, an interaction between quarks appears. Starting from these ideas, Diakonov has deduced an effective partition function of the form [12]

$$Z = \int \mathcal{D}\pi^A \int \mathcal{D}\psi^+ \mathcal{D}\psi \exp \left\{ \int d^4x \psi^+(x) \right. \\ \left. \times [i\gamma^\mu \partial_\mu + iM e^{i\gamma_5 \vec{\tau} \cdot \vec{\phi}/f_\pi}] \psi(x) \right\} \quad (1)$$

from which an effective quark Lagrangian can be obtained

$$\mathcal{L} = \overline{\psi}_f^\alpha (i\gamma^\mu \partial_\mu - M(q^2) e^{i\gamma_5 \vec{\tau} \cdot \vec{\phi}/f_\pi}) \psi_g^\alpha, \quad (2)$$

where  $\psi_f^\alpha$  is the quark spinor,  $\alpha$  is the color index,  $f$  and  $g$  are flavor indices, and  $M(q^2)$  is the dynamical mass of the quarks. Based on this Lagrangian, different models for the nucleon have been developed. For example, Diakonov *et al.* [13] describe the nucleon as a soliton solution, giving rise to the *chiral quark soliton model*. A similar approach can be found in Manohar and Georgi [14].

Although attractive from the theoretical point of view, chiral solitons are complicated to adopt for the derivation of the baryon-baryon interaction. For this reason, we will use here a simpler approach for the description of baryons and baryon-baryon interactions. Starting from the Hamiltonian originating from Eq. (2),

$$\mathcal{H}_{ch} = M(q^2) \bar{\psi}_f^\alpha e^{i\gamma_5 \vec{\tau} \cdot \vec{\phi}/f_\pi} \psi_g^\alpha \quad (3)$$

and with the philosophy of the linear sigma model,

$$\begin{aligned} \vec{\pi} &= \hat{\phi} f_\pi \sin(\phi/f_\pi), \\ \sigma &= f_\pi [\cos(\phi/f_\pi) - 1], \end{aligned} \quad (4)$$

one takes into account that the first term in the exponential series of Eq. (3) produces the quark constituent mass, and obtains the interacting Hamiltonian:

$$\mathcal{H}_{ch} \approx g_{ch} F(q^2) \bar{\psi}(\sigma + i\gamma_5 \vec{\tau} \cdot \vec{\pi}) \psi, \quad (5)$$

where  $g_{ch} = m_q/f_\pi$ ,  $F(q^2) = M(q^2)/M(0)$ , and  $m_q = M(0)$ . Hence, a scalar and a pseudoscalar field arise as a consequence of the chiral symmetry breaking. Here,  $F(q^2)$  is an unknown function which suppresses the chiral fields in the energy region where chiral symmetry is exact. It will be approximated by

$$F(q^2) = \left[ \frac{\Lambda_{\chi SB}^2}{\Lambda_{\chi SB}^2 + q^2} \right]^{1/2}, \quad (6)$$

where, as stated above,  $\Lambda_{\chi SB}$  determines the scale at which chiral symmetry is broken, and its value ranges between 600 MeV and 1 GeV.

Hence, it is straightforward to write the nonrelativistic potentials generated in the static approximation in the following way:

$$V_{ij}^{PS}(\vec{q}) = - \frac{1}{(2\pi)^3} \frac{g_{ch}^2}{4m_q^2} \frac{\Lambda_{\chi SB}^2}{\Lambda_{\chi SB}^2 + q^2} \frac{(\vec{\sigma}_i \cdot \vec{q})(\vec{\sigma}_j \cdot \vec{q})}{m_{PS}^2 + q^2} (\vec{\tau}_i \cdot \vec{\tau}_j), \quad (7)$$

$$V_{ij}^S(\vec{q}) = - \frac{g_{ch}^2}{(2\pi)^3} \frac{\Lambda_{\chi SB}^2}{\Lambda_{\chi SB}^2 + q^2} \frac{1}{m_S^2 + q^2}, \quad (8)$$

where  $\vec{q}$  is the three-momentum transfer, the  $\sigma$ 's ( $\tau$ 's) are the spin (isospin) Pauli matrices, and  $m_q$ ,  $m_{PS}$ , and  $m_S$  are the masses of the quark, pseudoscalar, and scalar bosons, respectively. The potentials refer to momentum states normalized to 1.

It is well established that the  $NN$  interaction at long-range is governed by pseudoscalar exchanges, namely the one-pion exchange (OPE) interaction. Therefore, if one wants to reproduce accurately this piece of the  $NN$  interaction, one is forced to identify the mass of the pseudoscalar field with the physical pion mass. The mass of the scalar field is obtained by the chiral relation [15]

$$\begin{aligned} m_{PS}^2 &= m_\pi^2, \\ m_S^2 &= m_{PS}^2 + 4m_q^2. \end{aligned} \quad (9)$$

If we also introduce the QCD perturbative effects, which mimic the gluon fluctuations around the instanton vacuum, the one-gluon exchange (OGE) potential arises and can be expressed as [16],

$$\begin{aligned} V_{ij}^{OGE}(\vec{q}) &= \frac{1}{(2\pi)^3} \frac{1}{4} (\vec{\lambda}_i \cdot \vec{\lambda}_j) 4\pi\alpha_s \\ &\times \left\{ \frac{1}{q^2} - \frac{1}{4m_q^2} \left( 1 + \frac{2}{3} (\vec{\sigma}_i \cdot \vec{\sigma}_j) \right) \right. \\ &\left. + \frac{1}{4m_q^2} \frac{1}{q^2} [\vec{q} \otimes \vec{q}]^2 \cdot [\vec{\sigma}_i \otimes \vec{\sigma}_j]^2 \right\}, \quad (10) \end{aligned}$$

where the  $\lambda$ 's are the color Gell-Mann matrices and  $\alpha_s$  is the strong-coupling constant.

The other QCD nonperturbative effect corresponds to confinement, and takes into account that the only observed hadrons are color singlets. It is phenomenologically introduced as a harmonic oscillator potential or as a linear potential. Confinement influences the spectrum, but its  $\vec{\lambda}_i \cdot \vec{\lambda}_j$  structure prevents contributions to the baryon-baryon interaction [17].

It is worth noticing that the scalar and the one-gluon exchange interactions contain spin-orbit terms. In Ref. [18], it was shown that, while these terms provide an important part of the spin-orbit force between nucleons, they are not enough to explain the experimentally observed effects. The situation of the spin-orbit force in quark-model potentials is still quite controversial [19], mainly due to our ignorance of the confinement mechanism. Contributions which are usually neglected (antisymmetric spin-orbit terms, Thomas precession terms, etc.) are even more important than those considered. Therefore, as not to obscure the discussion, we will postpone the study of this particular aspect of the interaction to a future work.

As we will use RGM to study the  $NN$  problem, we will make the usual ansatz for the radial wave function of the quarks,

$$\psi(\vec{r}_i) = \prod_{i=1}^3 \left[ \frac{1}{\pi b^2} \right]^{3/4} e^{-r_i^2/2b^2}, \quad (11)$$

so that the size of the baryon is fixed by  $b$ . One could argue that, once a quark-quark potential has been determined, the quark wave function of the three-quark clusters (baryons) should be obtained by solution of the Schrödinger equation. This process was carried out in Ref. [20], but the obtained wave functions are rather complicated for application to the calculation of the RGM kernels. However, in the same work [20], it was also shown that the  $NN$  potential obtained in the Born-Oppenheimer approach with these wave functions is very similar to the one obtained with Gaussian wave functions for a certain value of the parameter  $b$ . This legitimizes the Gaussian approach for low-energy  $NN$  scattering.

The wave function in momentum space corresponds to the Fourier transform of Eq. (11),

$$\psi(\vec{p}_i) = \prod_{i=1}^3 \left[ \frac{b^2}{\pi} \right]^{3/4} e^{-b^2 p_i^2/2}. \quad (12)$$

The baryon total wave function must include the spin, iso-spin, and color degrees of freedom, and will be denoted by

$$\begin{aligned} \psi_B &= \phi_B(\vec{p}_{\xi_1}, \vec{p}_{\xi_2}) \chi_B \xi_c[1^3]; \\ \phi_B(\vec{p}_{\xi_1}, \vec{p}_{\xi_2}) &= \left[ \frac{2b^2}{\pi} \right]^{3/4} e^{-b^2 p_{\xi_1}^2} \left[ \frac{3b^2}{2\pi} \right]^{3/4} e^{-(3b^2/4)p_{\xi_2}^2}, \end{aligned} \quad (13)$$

where  $\phi_B(\vec{p}_{\xi_1}, \vec{p}_{\xi_2})$  takes into account the internal spatial baryon degrees of freedom and is obtained from Eq. (12) by removing the center-of-mass wave function. Also,  $\chi_B$  labels the totally symmetric spin-isospin wave function coupled to the quantum numbers of the baryon  $B$ , and  $\xi_c[1^3]$  is the color singlet wave function. Built this way,  $\psi_B$  is totally antisymmetric in quark exchanges.

### III. THE RESONATING GROUP METHOD FOR THE TWO-BARYON SYSTEM IN MOMENTUM SPACE

In order to formulate RGM for the  $B_1 B_2$  system, we first need to determine the two-baryon wave function. Starting from the one-baryon wave function given by Eq. (13), the two-baryon wave function is taken to be the product  $\psi_{B_1} \psi_{B_2}$  coupled to the corresponding baryonic quantum numbers and multiplied by a wave function which takes into account the relative motion of the two baryons, here denoted as  $\chi(\vec{P})$ . Since the baryons are made up by fermions (quarks), the system should be in a totally antisymmetric state; therefore the two-baryon wave function is finally written as

$$\begin{aligned} \psi_{B_1 B_2} &= \mathcal{A}[\chi(\vec{P}) \psi_{B_1 B_2}^{ST}] \\ &= \mathcal{A}[\phi_{B_1}(\vec{p}_{\xi_{B_1}}) \phi_{B_2}(\vec{p}_{\xi_{B_2}}) \chi(\vec{P}) \chi_{B_1 B_2}^{ST} \xi_c[2^3]]. \end{aligned} \quad (14)$$

Here,  $\mathcal{A}$  is the antisymmetrizer of the six-quark system,  $\phi_{B_i}(\vec{p}_{\xi_{B_i}})$  is the internal spatial wave function defined in Eq. (13),  $\chi_{B_1 B_2}^{ST}$  denotes the spin-isospin wave function of baryons  $B_1$  and  $B_2$  coupled to a total spin-isospin ST, and  $\xi_c[2^3]$  is the product of the two color singlets.

As the one-baryon wave functions are already antisymmetrized, the antisymmetrizer may be written as  $\mathcal{A} = \frac{1}{2}(1 - P)(1 - 9P_{36})$ , where  $P_{36}$  is the operator that exchanges quarks 3 and 6 between the two clusters, and  $P = P_{14} P_{25} P_{36}$  is the operator that exchanges all the quarks between the two baryons. The operator  $\frac{1}{2}(1 - P)$  fixes the symmetry  $\mu$  of the wave function at the baryonic level. It was shown in Ref. [21] that this operator is properly taken into account by writing the wave function as

$$\begin{aligned} \psi_{B_1 B_2}^{\mu J L S T C} &= \frac{1}{\sqrt{2(1 + \delta_{B_1 B_2})}} \\ &\times [\psi_{B_1 B_2}^{J L S T C} + (-1)^{\mu + S_1 + S_2 - S + T_1 + T_2 - T} \psi_{B_2 B_1}^{J L S T C}] \end{aligned} \quad (15)$$

provided that

$$L + \mu = \text{odd}. \quad (16)$$

We will call symmetric the combination with  $\mu$  even, and antisymmetric that of  $\mu$  odd. Thus, the antisymmetrizer reduces to  $\mathcal{A} = (1 - 9P_{36})$ .

We also need to introduce the Schrödinger equation which governs the dynamics of the system. We write it as a projection equation

$$(\mathcal{H} - E_T)|\psi\rangle = 0 \Rightarrow \langle \delta\psi | (\mathcal{H} - E_T) |\psi\rangle = 0, \quad (17)$$

where

$$\mathcal{H} = \sum_{i=1}^N \frac{\vec{p}_i^2}{2m_q} + \sum_{i < j} V_{ij} - T_{\text{c.m.}} \quad (18)$$

with  $T_{\text{c.m.}}$  being the center-of-mass kinetic energy,  $V_{ij}$  is the interaction described in the previous section, and  $m_q$  is the constituent quark mass.

In Eq. (17), the variations are performed on the unknown relative wave function  $\chi(\vec{P})$ . In order to take it outside the antisymmetrizer, we introduce a continuous parameter  $\vec{P}_i$

$$\begin{aligned} \langle \vec{p}_{\xi_A} \vec{p}_{\xi_B} \vec{P} \vec{P}_{\text{c.m.}} | \psi \rangle &= \int \mathcal{A}[\phi_A(\vec{p}_{\xi_A}) \phi_B(\vec{p}_{\xi_B}) \delta^3(\vec{P} - \vec{P}_i)] \\ &\times \chi(\vec{P}_i) d\vec{P}_i, \end{aligned} \quad (19)$$

where we have only considered the spatial degrees of freedom in order to simplify the equations. Putting coordinates into the projection equation, we proceed as in Ref. [22] (changing the radial coordinate  $R$  into the momentum  $P$ , and keeping in mind that some operators are not diagonal in momentum space) in order to integrate out all the internal degrees of freedom of the clusters. Hence, we write the projected Schrödinger equation for the relative wave function as follows:

$$\begin{aligned} \left( \frac{\vec{P}'^2}{2\mu} - E \right) \chi(\vec{P}') + \int (\text{RGM} V_D(\vec{P}', \vec{P}_i) \\ + \text{RGM} K(\vec{P}', \vec{P}_i)) \chi(\vec{P}_i) d\vec{P}_i = 0, \end{aligned} \quad (20)$$

where  $E = E_T - E_A - E_B$  is the relative energy of the clusters, and  $\text{RGM} V_D(\vec{P}', \vec{P}_i)$  and  $\text{RGM} K(\vec{P}', \vec{P}_i)$  are the direct potential and the exchange kernel, respectively given by,

$$\begin{aligned} \text{RGM}V_D(\vec{P}', \vec{P}_i) = & \sum_{i \in A, j \in B} \int \phi_A^*(\vec{p}_{\xi'_A}) \phi_B^*(\vec{p}_{\xi'_B}) V_{ij}(\vec{P}', \vec{P}_i) \\ & \times \phi_A(\vec{p}_{\xi_A}) \phi_B(\vec{p}_{\xi_B}) d\vec{p}_{\xi'_A} d\vec{p}_{\xi'_B} d\vec{p}_{\xi_A} d\vec{p}_{\xi_B} \end{aligned} \quad (21)$$

and

$$\text{RGM}K(\vec{P}', \vec{P}_i) = \text{RGM}H_E(\vec{P}', \vec{P}_i) - E_T \text{RGM}N_E(\vec{P}', \vec{P}_i) \quad (22)$$

with

$$\begin{aligned} \text{RGM}H_E(\vec{P}', \vec{P}_i) = & -9 \int d\vec{p}_{\xi'_A} d\vec{p}_{\xi'_B} d\vec{p}_{\xi_A} d\vec{p}_{\xi_B} d\vec{P} \\ & \times \phi_A^*(\vec{p}_{\xi'_A}) \phi_B^*(\vec{p}_{\xi'_B}) \\ & \times \mathcal{H}P_{36}[\phi_A(\vec{p}_{\xi_A}) \phi_B(\vec{p}_{\xi_B}) \delta^3(\vec{P} - \vec{P}_i)]. \end{aligned} \quad (23)$$

A similar expression can be found for the normalization exchange kernel, replacing  $\mathcal{H}$  with the identity operator. The calculation of these kernels is detailed in the Appendix. Equation (20) is readily generalized to a coupled-channel equation, starting from a sum of wave functions of the type of Eq. (14) for the different baryon channels considered.

The RGM equations have usually been solved by means of a variational method developed by Kamimura [23]. With this method, the relative wave function is expanded in a Gaussian basis, so that the integrodifferential equations reduce to a matricial set of equations in the coefficients of the expansion. We here formulate an alternative method for the solution of coupled-channel RGM equations, deriving from Eq. (20) a set of coupled Lippmann-Schwinger equations of the form

$$\begin{aligned} T_\alpha^{\alpha'}(z; p', p) = & V_\alpha^{\alpha'}(p', p) + \sum_{\alpha''} \int dp'' p''^2 V_{\alpha''}^{\alpha'}(p', p'') \\ & \times \frac{1}{z - E_{\alpha''}(p'')} T_\alpha^{\alpha''}(z; p'', p), \end{aligned} \quad (24)$$

where  $\alpha$  labels the group of quantum numbers  $B_1 B_2 J L S T$  which defines a certain partial wave,  $V_\alpha^{\alpha'}(p', p)$  is the projected potential that contains the direct potential and the RGM exchange kernels, and  $E_{\alpha''}(p'')$  is the energy corresponding to a momentum  $p''$ , written as (in the nonrelativistic case):

$$E_\alpha(p) = \frac{p^2}{2\mu_\alpha} + \Delta M_\alpha. \quad (25)$$

Here,  $\mu_\alpha$  is the reduced mass of the  $B_1 B_2$  system corresponding to the channel  $\alpha$ , and  $\Delta M_\alpha$  is the difference between the threshold of the  $B_1 B_2$  system and the one we take as a reference, the  $NN$  system. The mass difference  $\Delta M_\alpha$  is obtained from the interaction terms for quarks belonging to

the same baryon, which relate to the total energy of the system  $E_T$  and to the relative energy between clusters  $E$ .

We solve the coupled-channel Lippmann-Schwinger equation using the matrix-inversion method proposed in Ref. [24], generalized in order to include channels with different thresholds. Once the  $T$  matrix is calculated, we determine the on-shell part, which is directly related to the scattering matrix. The relationship depends on the type of kinematics being used and, in the case of nonrelativistic kinematics,

$$S_\alpha^{\alpha'} = 1 - 2\pi i \sqrt{\mu_\alpha \mu_{\alpha'}} k_\alpha k_{\alpha'} T_\alpha^{\alpha'}(E + i0^+; k_{\alpha'}, k_\alpha) \quad (26)$$

with  $k_\alpha$  defined by

$$k_\alpha^2 = 2\mu_\alpha(E - \Delta M_\alpha), \quad (27)$$

so that, for channels above the threshold,  $k_\alpha^2 > 0$ .

If inelastic channels are not considered, the scattering matrix must be unitary. Therefore, if there is only one channel above the threshold, the scattering matrix is directly parametrized in terms of the phase shift. In the case of two coupled channels, the parametrization is not unique and we will use that of Stapp *et al.* [25].

For bound states, the integral equations do not have poles and the problem is simplified. Using the same discretization method as in the Lippmann-Schwinger equation problem, the Schrödinger equation can be written in the form

$$\sum_j [E_i(p_i) \delta_{ij} + V_{ij} - E \delta_{ij}] \psi_j = 0, \quad (28)$$

where  $i$  and  $j$  label the discretization of the integral and the quantum numbers of the different channels included in the calculation, and  $\psi_j$  is the value of the wave function in the channel and momentum corresponding to the index  $j$ .

In general, the matrix elements  $V_{ij}$  do not depend on energy and it is sufficient to solve Eq. (28) as an eigenvalue problem, with the negative solutions corresponding to the energies of the bound states. In the case of the RGM method, the matrix elements  $V_{ij}$  depend on  $E$  through the dependence of the exchange kernels. For this reason, we should first fix the zeros of the Fredholm determinant by solving

$$|E_i(p_i) \delta_{ij} + V_{ij} - E \delta_{ij}| = 0 \quad (29)$$

with the zeros being the energies of the bound states. Once we know these energies, Eq. (28) is solved for each value, and the wave function of the bound state is the eigenvector corresponding to the eigenvalue that coincides with the binding energy.

#### IV. MODEL PARAMETERS

A rough estimate of the values of the model parameters can be done based on the following arguments. As the pseudoscalar field is identified at long-range with the pion, the  $g_{ch}$  coupling constant should reproduce in an accurate way the long-range interaction given by the OPE. If the two nucleons are separated enough, the central part of the pseudoscalar interaction between quarks given by Eq. (7) gener-

TABLE I. Model parameters.

$b(\text{fm})$	0.518
$m_q(\text{MeV})$	313
$\Lambda_{\chi SB}(\text{fm}^{-1})$	4.2997
$m_{PS}(\text{fm}^{-1})$	0.7
$g_{ch}^2$	6.6608
$\alpha_s$	0.4977
$m_S(\text{fm}^{-1})$	3.513

ates an interaction between nucleons of the form

$$V_c^{PS}(r) = \frac{1}{3} \frac{g_{ch}^2}{4\pi} \frac{m_\pi^2}{4m_q^2} \tilde{\rho}(im_\pi)^2 \frac{e^{-m_\pi r}}{r} \left(\frac{5}{3}\right)^2 (\vec{\sigma}_N \cdot \vec{\sigma}_N)(\vec{\tau}_N \cdot \vec{\tau}_N), \quad (30)$$

where  $\tilde{\rho}(q)$  is the quark density Fourier transform of each nucleon normalized to  $\tilde{\rho}(q=0)=1$ . Comparing with the standard OPE Yukawa potential,

$$V_c^{OPE}(r) = \frac{1}{3} \frac{f_{\pi NN}^2}{4\pi} \frac{e^{-m_\pi r}}{r} (\vec{\sigma}_N \cdot \vec{\sigma}_N)(\vec{\tau}_N \cdot \vec{\tau}_N) \quad (31)$$

and using  $\tilde{\rho}(q) = e^{-b^2 q^2/6}$ , one finally obtains

$$\frac{g_{ch}^2}{4\pi} = \left(\frac{3}{5}\right)^2 \frac{f_{\pi NN}^2}{4\pi} \frac{4m_q^2}{m_\pi^2} e^{-b^2 m_\pi^2/3}. \quad (32)$$

This gives the chiral coupling constant  $g_{ch}$  in terms of the  $\pi NN$  coupling constant, taken to be  $f_{\pi NN}^2/4\pi = 0.0749$  [26].

As previously mentioned, the parameter  $b$  determines the size of the nucleon quark content, and should not be confused with the nucleon charge radius. Usual values range between 0.4 and 0.6 fm, and we will here take  $b = 0.518$  fm. This value was obtained by comparing the Born-Oppenheimer  $NN$  potential (calculated from the wavefunction solution of the bound-state problem for the Hamiltonian described in Sec. II) to the  $NN$  potential calculated with a single Gaussian of parameter  $b$ .

$\Lambda_{\chi SB}$  controls the pion-gluon proportion in the model and, as a consequence, it controls the strength of the tensor force,

which is mainly due to the pion interaction. In order to fix the value of  $\Lambda_{\chi SB}$ , one needs to examine a process dominated by the pion tensor term. Such a reaction may be the  $pp \rightarrow n\Delta^{++}$  because, at high momenta, more than 90% of the interaction corresponds to the pion tensor part. The calculation of Ref. [27] suggests a value close to  $4.2 \text{ fm}^{-1}$  for  $\Lambda_{\chi SB}$ .

The value of  $\alpha_s$  is estimated by means of the  $N-\Delta$  mass difference, which has been traditionally explained in terms of the OGE. In the model presented here, however, there are contributions not only from OGE, but also from the pseudoscalar piece of the interaction, the latter contributing approximately half of the total mass difference. The rest is attributed to the OGE, and the value of  $\alpha_s$  is adjusted to reproduce the experimental  $N-\Delta$  mass difference.

The values of the parameters are finally fine tuned in order to reproduce the binding energy of the deuteron in presence of the coupling to  $\Delta\Delta$  channels. The parameters used in the present calculations are quoted in Table I.

## V. BOUND-STATE PROBLEM: THE DEUTERON

Traditionally, the deuteron has been understood as a  $J^\pi = 1^+$  two-nucleon system, thus corresponding to an isospin singlet in even partial waves (i.e.,  $^3S_1$  and  $^3D_1$ ). However, it could also be described as a linear combination of pairs of baryonic resonances, provided the resonances have the same isospin to ensure that the total isospin is zero. The presence of color through the quark model in the hadron dynamics adds the possibility of new exotic components, such as the *hidden color* states. They correspond to two color octets coupled to a singlet. In some works, their contribution to the deuteron wave function was estimated and found to be as large as 5% [28], i.e., the same order of magnitude of the deuteron  $D$  component. However, it is possible to demonstrate [29] that any *hidden color* state can always be expressed as a linear combination of physical states given by Eq. (13).

Since the deuteron is the only bound two-nucleon system, there has been much experimental and theoretical work concerning the presence of other components, mainly isobars, in addition to the two nucleons. We will assume that the deuteron can be described as configurations of two clusters

TABLE II. Probability of the different deuteron components. The symbol  $\times$  indicates that the partial wave is not included in the calculation. In calculation 8, a multiplicative factor in the scalar potential is introduced as explained in the text.

	$^3S_1^{NN}$ (%)	$^3D_1^{NN}$ (%)	$^3S_1^{\Delta\Delta}$ (%)	$^3D_1^{\Delta\Delta}$ (%)	$^7D_1^{\Delta\Delta}$ (%)	$^7G_1^{\Delta\Delta}$ (%)	$E_D(\text{MeV})$
1	95.1989	4.5606	0.1064	0.0035	0.1243	0.0063	-2.2246
2	96.3966	3.6034	$\times$	$\times$	$\times$	$\times$	-1.0234
3	96.0860	3.8340	0.0800	$\times$	$\times$	$\times$	-1.2114
4	96.3828	3.6156	$\times$	0.0029	$\times$	$\times$	-1.0356
5	95.6593	4.2332	$\times$	$\times$	0.1075	$\times$	-1.8353
6	96.2854	3.7104	$\times$	$\times$	$\times$	0.0042	-1.0685
7	95.3295	4.4451	0.1034	$\times$	0.1219	$\times$	-2.1327
8	95.3780	4.6220	$\times$	$\times$	$\times$	$\times$	-2.2246

TABLE III. Probability for the  $\Delta\Delta$  components in the deuteron compared to baryonic models: Arenhövel [33] and Dymarz and Khanna [34].

%	CQC	Ref. [33]	Ref. [34] ( $w/s$ )
${}^3S_1^{\Delta\Delta}$	0.1064	0.1700	0.340/0.13
${}^3D_1^{\Delta\Delta}$	0.0035	0.0500	0.040/0.03
${}^7D_1^{\Delta\Delta}$	0.1243	0.5100	0.100/0.38
${}^7G_1^{\Delta\Delta}$	0.0063	0.0500	0.005/0.02
Total	0.2405	0.7800	0.485/0.56

of three quarks. In order of increasing mass, the possible combinations are  $N(939)N(939)$ ,  $N(939)N^*(1440)$ ,  $\Delta(1232)\Delta(1232)$ , and  $N(939)N^*(1650)$ . From the energy point of view, the most important corrections to the deuteron  $NN$  wave function should come from the  $N(939)N^*(1440)$  configuration, being the one with the next lowest mass. Rost [30] obtained a 0.16% probability for this configuration. However, the uncertainties associated with the coupling constants of the transition potential make this number not very significant. Glozman *et al.* [31] have calculated the spectroscopic factors of the different configurations for the deuteron wave function corresponding to the Paris potential. Their estimate for the spectroscopic factor of the  $N(939)N^*(1440)$  configuration is  $S_{NN^*}^d < 10^{-3}$ . But, for the next mass configuration,  $\Delta(1232)\Delta(1232)$  with a mass of only about 60 MeV higher, the estimated factor was  $S_{\Delta\Delta}^d \sim 5 \times 10^{-2}$ , predicting this effect as more important than the  $N(939)N^*(1440)$ .

Taking into account that there are no experimental data on the  $N(939)N^*(1440)$  configuration [whereas, for the  $\Delta(1232)\Delta(1232)$  configuration, Allasia *et al.* [32] established a significant upper limit of about 0.4%], we will carry out a coupled-channel calculation including  $N(939)N(939)$  and  $\Delta(1232)\Delta(1232)$  components for partial waves with the deuteron quantum numbers. In particular, besides the  ${}^3S_1^{NN}$  and  ${}^3D_1^{NN}$  components, we will include the following  $\Delta\Delta$  components:  ${}^3S_1^{\Delta\Delta}$ ,  ${}^3D_1^{\Delta\Delta}$ ,  ${}^7D_1^{\Delta\Delta}$ , and  ${}^7G_1^{\Delta\Delta}$ .

In Table II, we show the contribution of each  $\Delta\Delta$  component to the deuteron binding energy. For the sake of comparison, we present a calculation including  $NN$  components only, and labeled as number 8. For this particular case, leaving out the  $\Delta\Delta$  components, we had to artificially increase the attraction by means of a multiplicative factor (1.0635) in the coupling constant of the scalar potential. As can be observed, the probability of  $\Delta\Delta$  components is very small. The probabilities of the  ${}^3S_1^{\Delta\Delta}$  and  ${}^7D_1^{\Delta\Delta}$  are by far the most im-

TABLE IV. Deuteron properties.

	Quark <sup>a</sup>	Quark <sup>b</sup>	OBEP [1]	Paris [35]	Expt. [36]
$E_D(\text{MeV})$	2.2246	2.2246	2.2246	2.2249	2.224575(9)
$r_m(\text{fm})$	1.985	1.976	1.9688	1.9717	1.971(6)
$A_s(\text{fm}^{-1/2})$	0.8941	0.8895	0.8860	0.8869	0.8846(8)
$\eta$	0.0250	0.0251	0.0264	0.0261	0.0256(4)

<sup>a</sup>Calculation 1 in Table II.

<sup>b</sup>Calculation 8 in Table II.

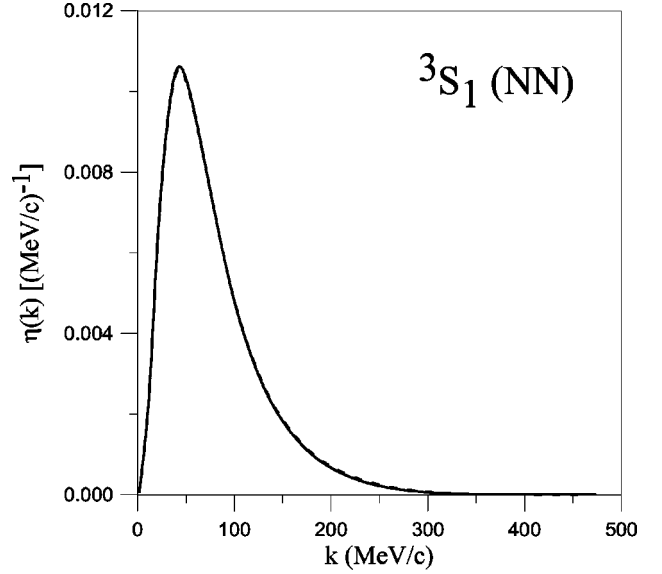


FIG. 1. Probability density  $\eta(k) = k^2|\Psi(k)|^2$  in momentum space for the  ${}^3S_1^{NN}$  deuteron component. The solid line represents the full calculation including  $\Delta\Delta$  channels. Dashed line corresponds to calculation 8 in Table II.

portant, due to their strong tensor couplings. This is in agreement with the results of baryonic models [33,34]. Besides, the total probability for  $\Delta\Delta$  components in the deuteron is compatible with the experimental limits given by Allasia *et al.* [32]. This is not the case for baryonic models. Thus, for example, Arenhövel [33] carried out a coupled-channel calculation using, for the  $NN \rightarrow \Delta\Delta$  transition potential, a combination of  $\pi$  and  $\rho$  exchanges, and the Reid soft core potential for the rest. Table III shows that, although the probabilities have the same distributions as ours, the total probability is three times larger than the one we obtained in our model. A similar comment could be made about the calculations of Dymarz and Khanna [34], where, in spite of the distributions being similar to ours, the total probability is twice as much. One must be aware that calculations at the baryonic level are not fully consistent, as they use, for the  $NN$  interaction, potentials (Reid soft core or Paris) which were designed, in principle, without explicit  $\Delta$  degrees of freedom: therefore, parts of the contributions from the  $\Delta$  degrees of freedom are implicitly included in the parametrization of the potentials.

In Table IV, we show some of the properties of the deuteron. A good agreement with the experimental data can be observed. The effect of the  $\Delta\Delta$  components on the mean-square radius is negligible  $\sim 0.01\%$ , due to the low probability of these components and to the fact that their contribution occurs fundamentally for small values of the radius  $r$ . A similar agreement can be obtained with nucleonic channels only (see column three). This result tells us that, for global properties, the influence of the  $\Delta\Delta$  channels can be simulated by a small change of the parameters (a multiplicative factor on the scalar potential). Nevertheless, as we will explain below, one has to keep in mind that these parameters are strongly correlated to the calculation of other observables, and therefore should not be freely modified.

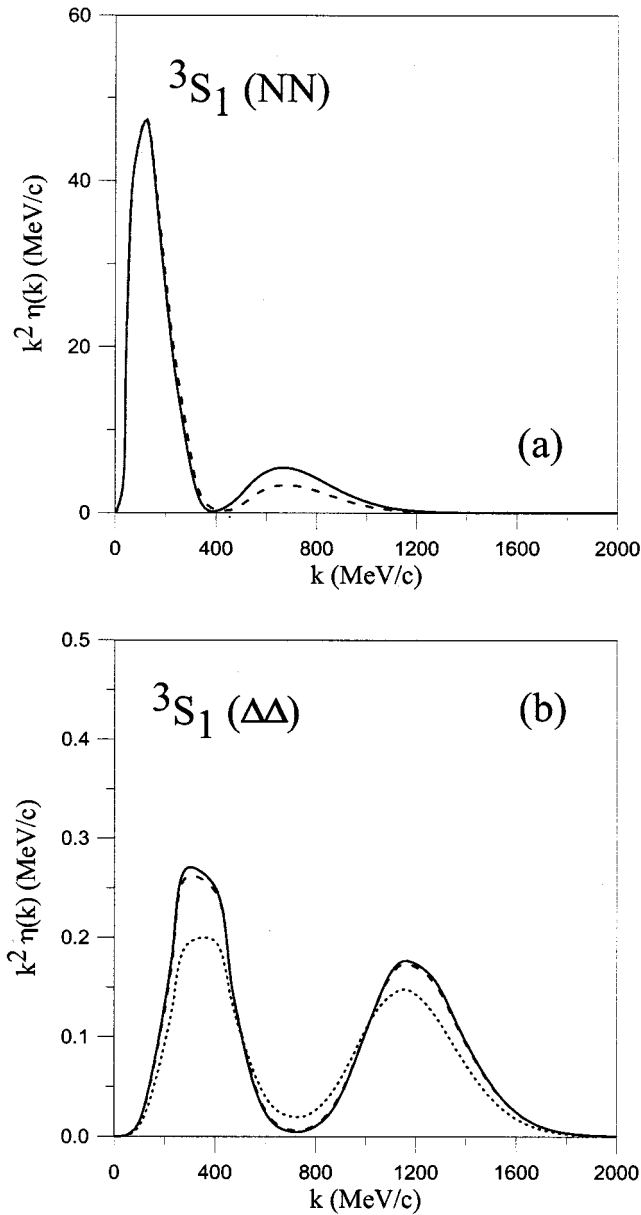


FIG. 2. Momentum distribution for the  ${}^3S_1^{NN}$  and  ${}^3S_1^{\Delta\Delta}$  deuteron components. (a) Solid and dashed lines are the same as in Fig. 1. (b) The solid line corresponds to the full calculation, dotted and dashed lines to calculations 3 and 7 in Table II.

Figure 1 shows the probability distribution in momentum space for the  ${}^3S_1^{NN}$  deuteron component: once again, it is seen that the effect of the  $\Delta\Delta$  components can be simulated by readjusting the strength of the scalar potential. However, this is not the case for the momentum distributions  $k^2\eta(k)$  which are shown in Fig. 2 for  $S$ -wave deuteron components. As can be observed, the  $\Delta\Delta$  components extend to higher momenta regions. This may influence the structure function  $B(q)$  which presents a zero for momentum at around  $7.1 \text{ fm}^{-1}$ . Including only  $NN$  components, this result always comes lower, being the  $\Delta\Delta$  components a possible candidate to solve the problem [34,37]. As a consequence, although the probability of  $\Delta\Delta$  components is small, its influence could

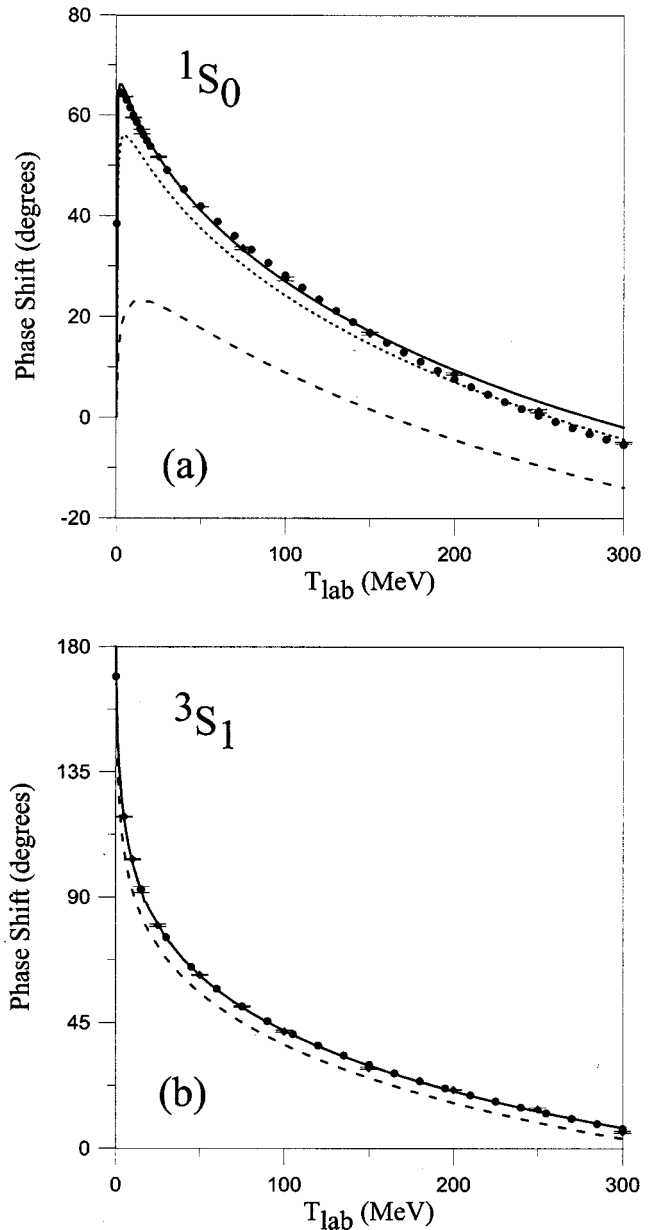


FIG. 3.  $NN$   $S$  wave phase shifts for  $T=1$  (a) and  $T=0$  (b). Experimental points with and without error bars correspond to the energy-independent and energy dependent solutions of Arndt *et al.* [38], respectively. All these data have been obtained through the interactive program SAID [39] corresponding to the solution SP98. The phase shifts shown and the analysis correspond to the neutron proton. (a) The dashed line represents the calculation including  $NN$  channels only, dotted line includes also  $N\Delta$  components, and solid line is the full calculation with  $NN$ ,  $N\Delta$ , and  $\Delta\Delta$  channels. (b) The dashed line is the calculation with  $NN$  only, and solid line is the full calculation including  $NN$  and  $\Delta\Delta$  channels.

be relatively important for certain specific aspects, and not so easily replaced by other mechanisms.

## VI. SCATTERING STATES PROBLEM: $NN$ PHASE SHIFTS

In this section, we present and discuss our results for the  $NN$  phase shifts below the pion threshold. In the calcula-

TABLE V. Low-energy scattering parameters.

	Quark	OBEP [1]	Paris [35]	Expt. [42]
$a_{np}$ (fm)	-27.010	-23.750	-17.612	-23.748(10)
$r_{np}$ (fm)	2.64	2.71	2.88	2.75(5)
$a_t$ (fm)	5.437	5.424	5.427	5.419(7)
$r_t$ (fm)	1.779	1.761	1.766	1.754(8)

tions, we will include couplings to  $\Delta\Delta$  channels for isosinglet ( $T=0$ ) partial waves, and to  $N\Delta$  and  $\Delta\Delta$  channels for isotriplet ( $T=1$ ) partial waves. As explained in the introduction, the CQC model provides a way to study the  $\Delta$  excitation for the  $NN$  elastic scattering in a completely parameter-free fashion. We will use as reference the experimental data of Arndt *et al.* [38]. All these data have been obtained through the interactive program SAID [39] corresponding to the solution SP98. The phase shifts shown and the analysis correspond to the neutron proton.

For the discussion of the results, we will divide the phase shifts into three groups. First, we will consider  $L=0$  waves. They are the most sensitive to the short-range part of the interaction: therefore, one would expect that quark dynamics play an important role. A second group will be  $P$ ,  $D$ , and  $F$  waves. They are still sensitive to the short-range part and therefore to quark dynamics, but the middle-range and the spin-orbit terms also play a dominant role. Finally, waves with orbital angular momentum  $L>3$  depend fundamentally on the middle and long-range part of the interaction. Quark dynamics should not be relevant, but these waves may be used to study the chiral component of the  $NN$  interaction. We will also present our results for the mixing parameters.

#### A. $S$ waves

In Fig. 3(a), we show the results for the  $^1S_0^{NN}$  partial wave. Angular momentum selection rules prevent this chan-

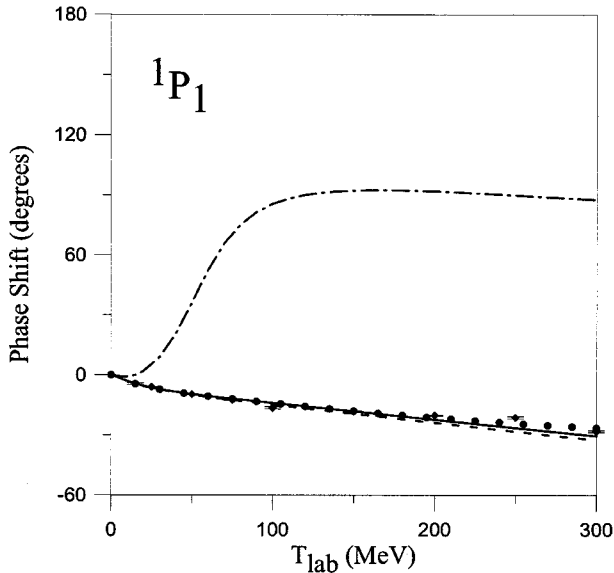


FIG. 4.  $NN$   $^1P_1$  phase shift. The dashed and solid lines have the same meanings as in Fig. 3(b). The dashed-dotted line shows the effect of antisymmetry, corresponding to the result when all the exchange kernels are removed.

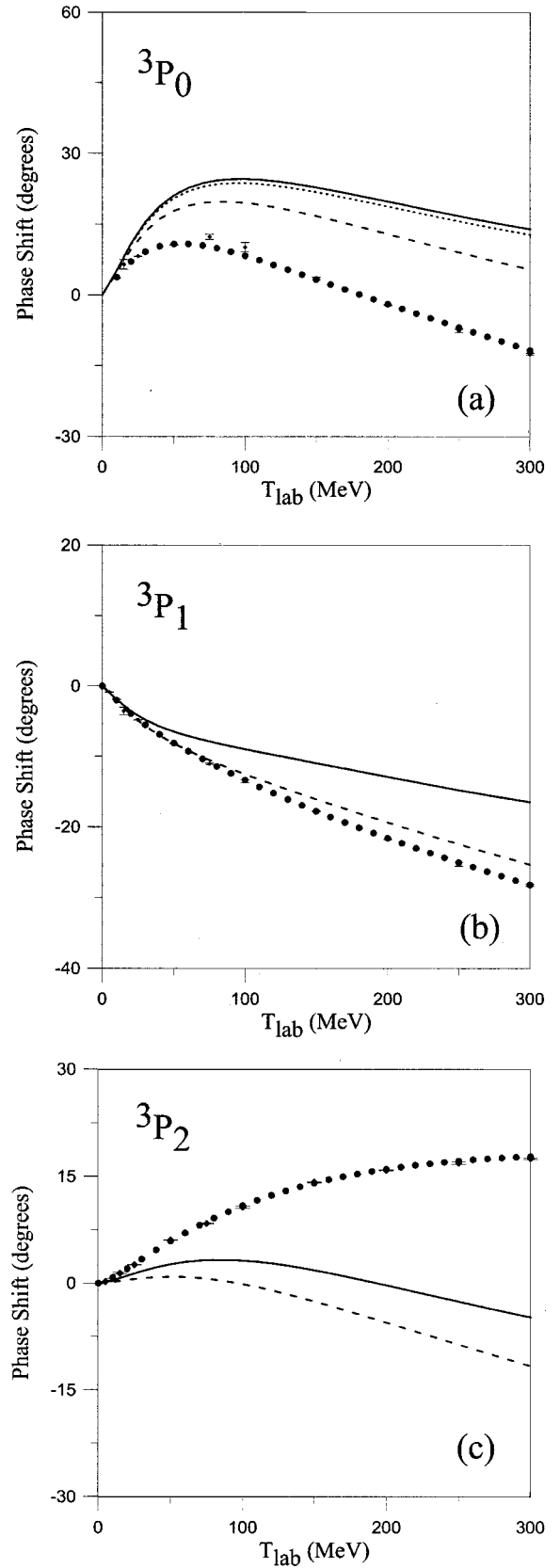


FIG. 5.  $NN$   $^3P_J$  phase shifts. (a) Same meaning as in Fig. 3(a). (b), (c) The dashed line corresponds to the result with  $NN$  channels only, and the solid line includes  $NN$  and  $N\Delta$  channels.

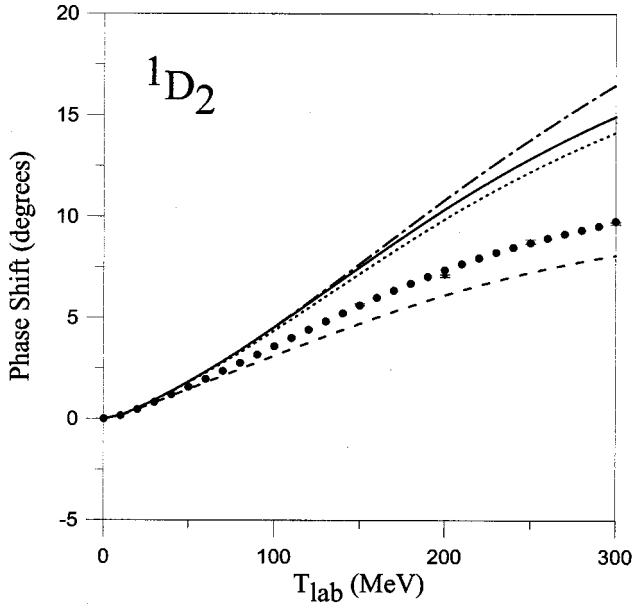


FIG. 6.  $NN$   $^1D_2$  phase shift. The solid, dashed, and dotted lines have the same meanings as in Fig. 3(a). The dashed-dotted line represents the result without exchange kernels.

nel from coupling to other  $NN$  channels. As pointed out before, the chiral components of the  $NN$  interaction do not provide enough attraction to reproduce the experimental data (dashed line). The required attraction is supplied by the coupling to the  $^5D_0^{N\Delta}$  channel (dotted line). A complete agreement with the experimental data is obtained when the coupling to  $\Delta\Delta$  channels is included (solid line). For the isotriplet partial waves, the effect of the coupling to  $\Delta\Delta$  channels is very small as shown here, and as will be also seen for higher angular momentum partial waves. Therefore, in order to simplify the calculations, we will simulate this coupling (which always translates into an additional attraction) by means of a small modification of the mass of the scalar potential for these channels. As a consequence, for the rest of the isotriplet partial waves, we will adopt a mass of  $3.421 \text{ fm}^{-1}$  for the scalar particle. This is the same value used in a recent study of the  $^1S_0$  partial wave [40], where we did not include  $\Delta\Delta$  channels. In Fig. 3(b), results corresponding to the deuteron quantum numbers are shown. The agreement with the experimental data is also good. The coupling to the  $\Delta\Delta$  channels (solid line) has a very small influence on the phase shift, showing that the important channels are those coupled by tensor potentials.

The short-range repulsion of the potential is very well reproduced without introducing any additional parameters. The presence of a pseudoscalar interaction reduces the value of  $\alpha_s$  in the OGE (the interaction usually advocated to explain the short-range repulsion of the  $NN$  potential), but Ref. [41] shows that antisymmetry effects on the pseudoscalar potential provide a strong spin-isospin independent repulsion, which allows us to reproduce the behavior of the  $S$ -wave phase shifts even in the absence of OGE.

We show in Table V the low-energy scattering parameters. The  $NN$  scattering length in the  $^1S_0$  state is extremely sensitive to small changes in the strength of the force as there

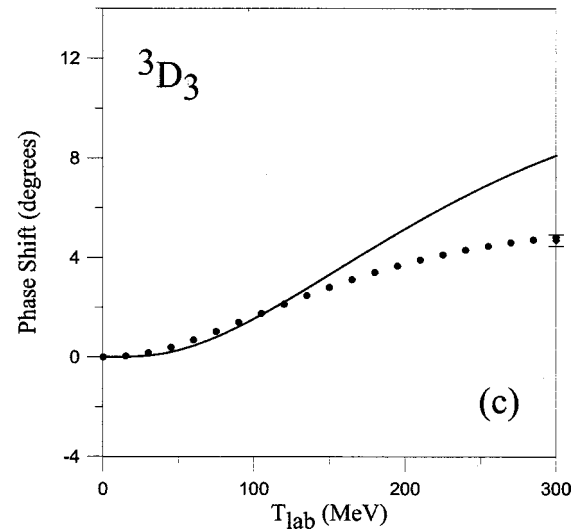
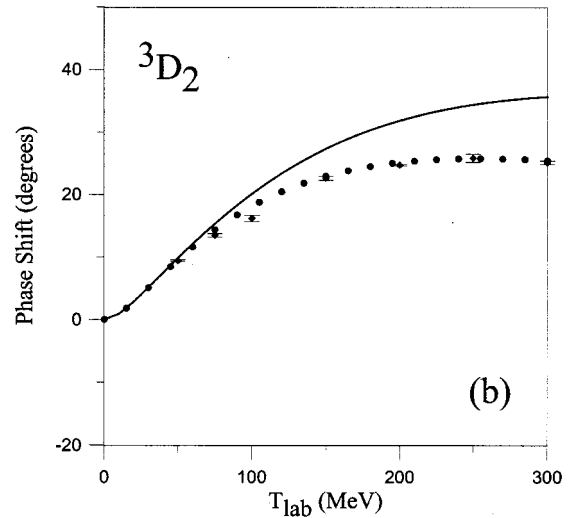
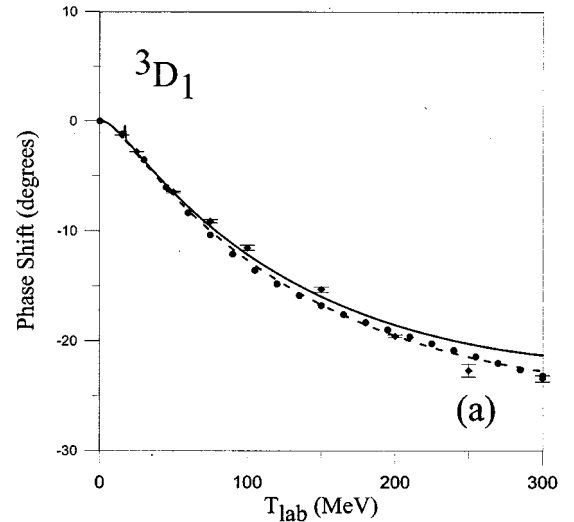


FIG. 7.  $NN$   $^3D_J$  phase shifts. (a) Lines are labeled as in Fig. 3(b). (b), (c) The solid line corresponds to the result with  $NN$  channels only.

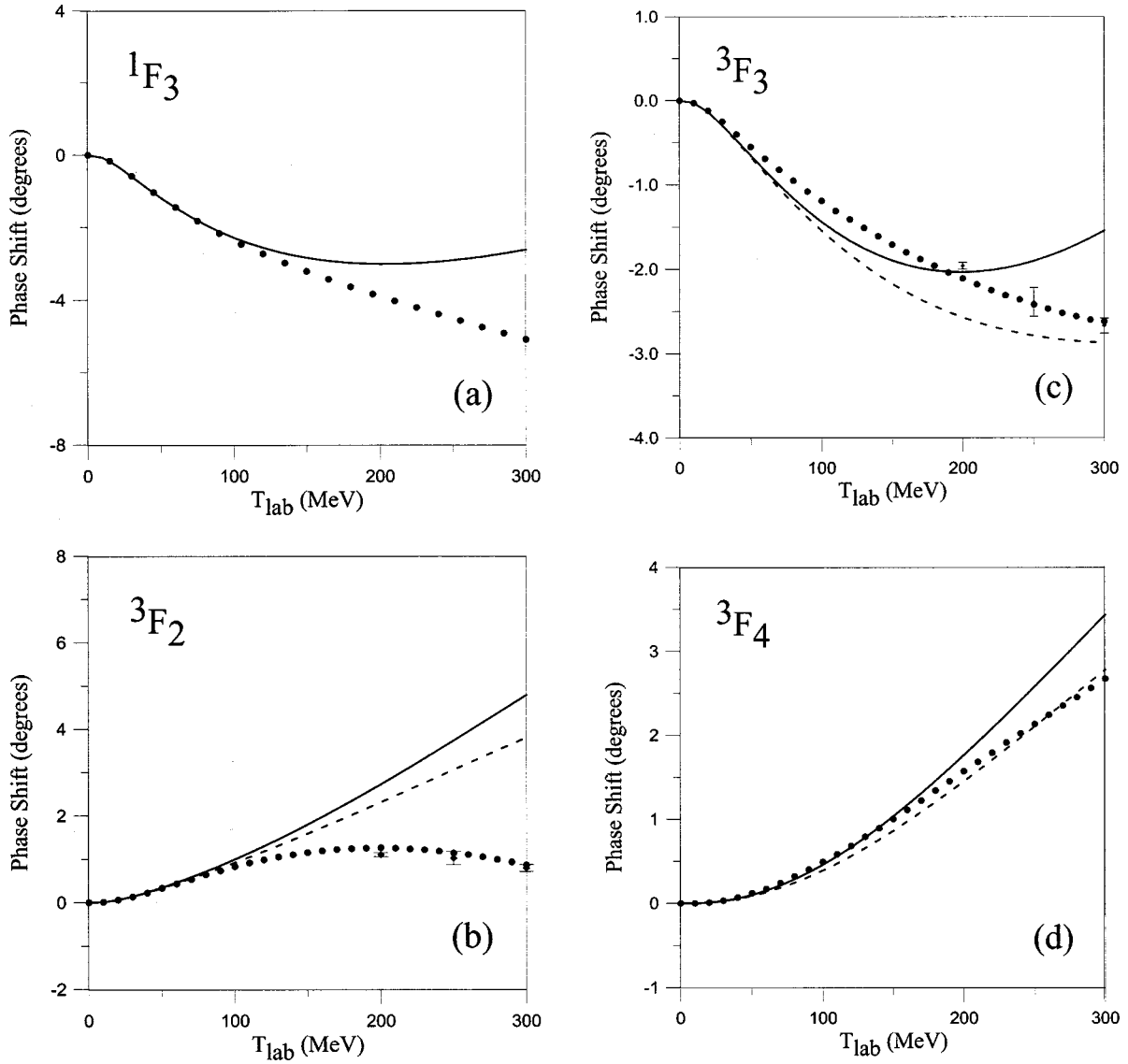


FIG. 8.  $NN$   $F$  phase shifts. In the  $T=0$  sector, the solid line includes  $NN$  channels only. In the  $T=1$  sector, the dashed line corresponds to including  $NN$  channels only, and the solid line considers also  $N\Delta$  channels.

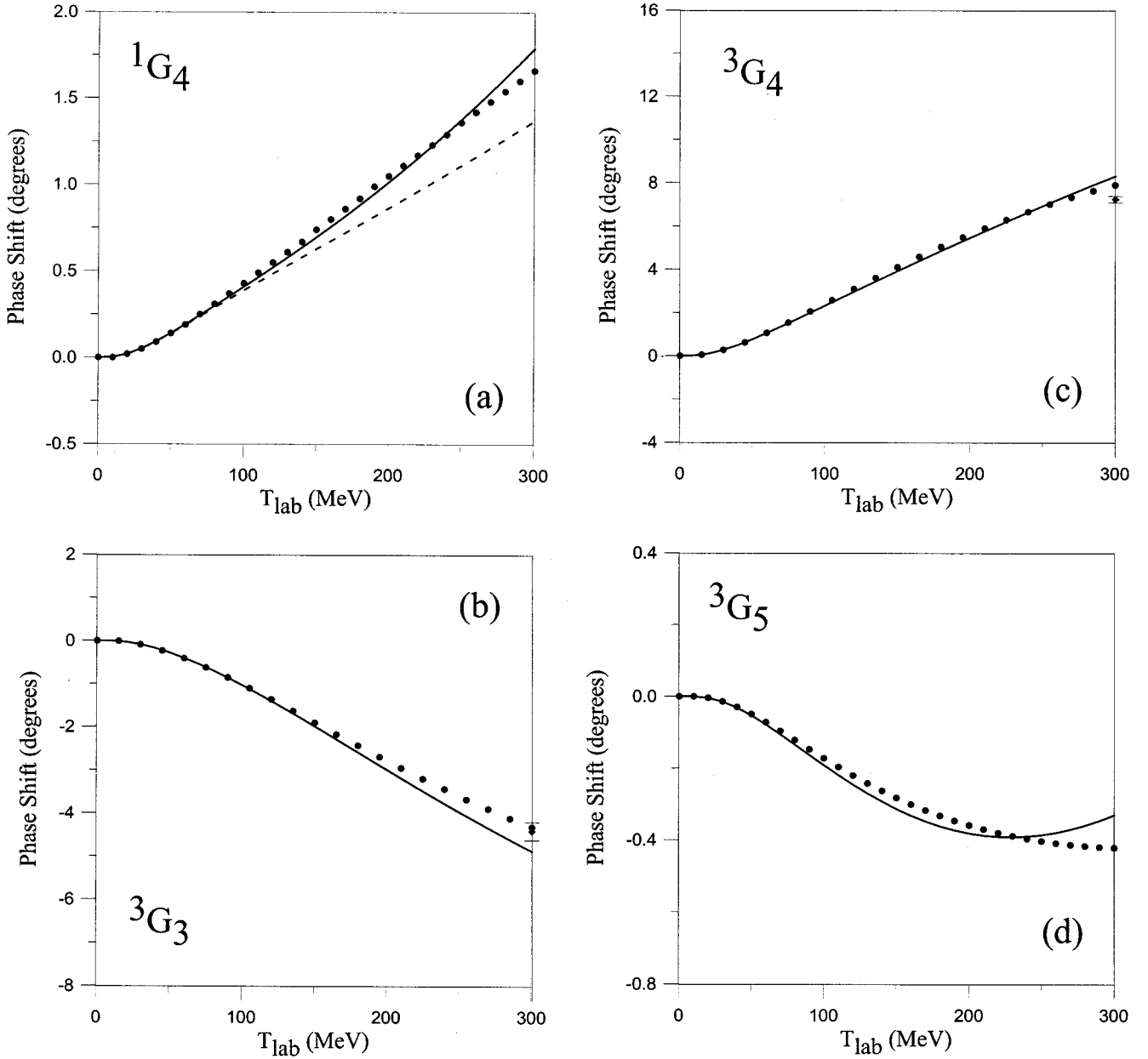
exists an almost bound state in this partial wave. A detailed discussion of the scattering length problem in the same model presented here (as mentioned above without including  $\Delta\Delta$  channels) has been done in Ref. [40]. One should be aware that the quark model results in Table V have been calculated with a unique set of parameters, without differentiating  $T=0$  and  $T=1$  channels. A nonsignificant modification on the mass of the scalar boson in the  $T=1$  channel will drive the exact result for this observable.

### B. $P$ , $D$ and $F$ waves

Among the four  $L=1$  waves, only the  $^1P_1$  is not affected by the spin-orbit interaction. As we can see in Fig. 4, the result of our calculation (corresponding to the solid line) is in perfect agreement with the experimental data. Let us note that this calculation, as well as all others that we will show next, is a parameter-free calculation, in the sense explained in Sec. III: that is, the model parameters of Table I are fitted

to different observables. It is also interesting to notice that, for the  $^1P_1$  partial wave, the quark substructure of the nucleon still plays an important role. Indeed, in the same figure, we denote by the dashed-dotted line the calculation done by removing the terms coming from the antisymmetry of the quarks, and the phase shift becomes attractive. This result is easily understood in terms of the pseudoscalar interaction (OGE does not contribute to  $P$  waves because of its  $\delta$ -like behavior). In fact, at short range, the direct pseudoscalar potential is repulsive for  $S$  waves, but is attractive for the  $^1P_1$  wave due to the sign change of the spin-isospin matrix element. Only the antisymmetry terms of the pseudoscalar potential produce this correct behavior.

In Fig. 5, the  $^3P_J$  triplet phase shifts are shown. As we can see in Fig. 5(a), and has been explained for  $S$  waves, the coupling to  $\Delta\Delta$  channels in higher angular momentum isotriplet partial waves is very small. A lack of spin-orbit interaction prevents an appropriate reproduction of the experi-

FIG. 9.  $NN$   $G$  phase shifts. Lines have the same meanings as in Fig. 8.

mental data. The coupling to  $N\Delta$  channels, suggested as a possible solution of the spin-orbit problem, does not improve the description.

$D$  waves are shown in Figs. 6 and 7. As a general trend, one observes that there is too much attraction, except for the  ${}^3D_1$  partial wave where the experimental data are perfectly reproduced. While for isotriplet partial waves  ${}^1D_2$  the coupling to  $N\Delta$  channels is still important (worsening the quality of the results), the coupling to  $\Delta\Delta$  channels does not produce any considerable effect. For this reason, the coupling to  $\Delta\Delta$  channels will not be included for higher isotriplet partial waves. We also notice that, for these waves, the influence of the antisymmetry diminishes as compared to  $S$  and  $P$  waves.

As in the case of Kaiser *et al.* [43], we observe how the  $D$  waves are correctly reproduced up to about 80–100 MeV,

which may be considered as the characteristic window where the  $NN$  interaction is basically governed by chiral symmetry. Higher energies require an improvement in the description of short-range effects, as could be the spin-orbit force which still plays an important role for  $D$  waves.

The phase shifts for  $F$  waves are shown in Fig. 8. We see how, in general, there is a better agreement than in  $D$  waves up to higher energies of 150–200 MeV. We have included again the calculation without coupling to  $N\Delta$  channels for isotriplet partial waves. As for  $P$  and  $D$  waves, the coupling to  $N\Delta$  channels produces too much attraction. An agreement is obtained of the same quality as the results reported in Refs. [5,43].

A comment must be made about the  ${}^3F_2$  phase shift. This wave is coupled to the  ${}^3P_2$  wave, which has a strong influence of the spin-orbit interaction. The spin-orbit interaction

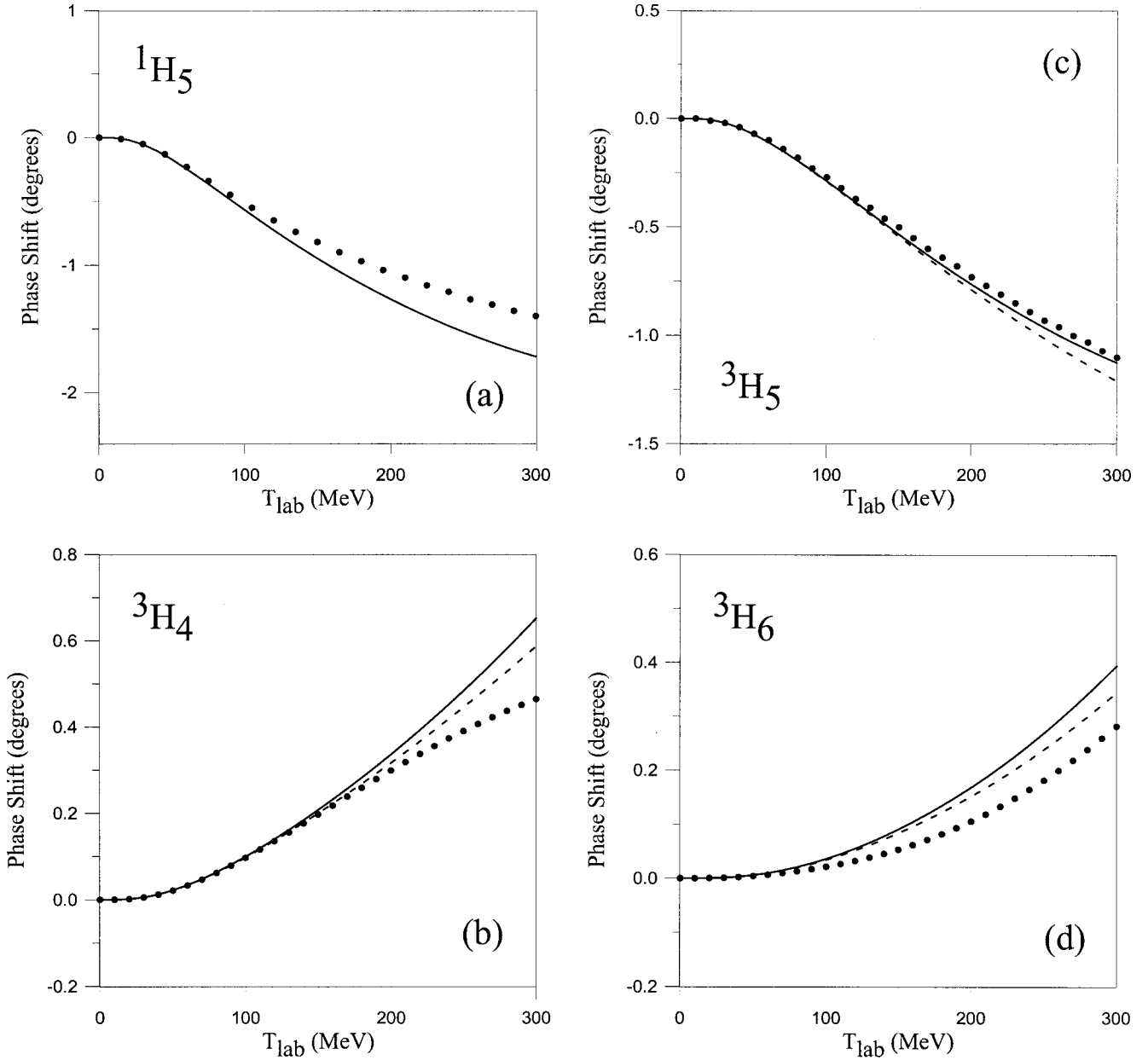


FIG. 10.  $NN$   $H$  phase shifts. Lines have the same meanings as in Fig. 8.

is attractive for the  ${}^3P_2$  wave and repulsive for the  ${}^3F_2$ . Therefore, we expect that when the  ${}^3P_2$  wave approaches the experimental data, the  ${}^3F_2$  will also do the same.

### C. $G$ , $H$ , and $I$ waves

In Figs. 9, 10, 11, and 12, we show the results for  $G$ ,  $H$ ,  $I$ , and  $J$  partial waves up to  $J=6$ . The predictions of the model are in good agreement with the experimental data, being fundamentally dominated by the interaction of chiral origin. Isotriplet partial waves show that the coupling to  $N\Delta$  channels, so important for low angular momenta, becomes smaller but contributes to improve the results.

For high angular momentum partial waves, our results are similar to those obtained by effective theories [5,43], indicating that these waves are governed exclusively by chiral sym-

metry. However, as previously discussed, the effective theories trying to reproduce low partial waves need to introduce a large number of parameters (more than 20 in Ref. [3]).

### D. Mixing parameters

Finally, we show in Fig. 13 the mixing parameters for the tensor couplings between different  $NN$  partial waves. As can be seen, all of them are correctly reproduced except for  $\epsilon_1$  (which represents the tensor coupling  ${}^3S_1-{}^3D_1$ ) and  $\epsilon_2$  (which represents the tensor coupling  ${}^3P_2-{}^3F_2$ ).

For  $\epsilon_2$ , we cannot draw any definite conclusions, because our model does not describe accurately the  ${}^3P_2$  and  ${}^3F_2$  partial wave phase shifts. However, for  $\epsilon_1$  [solid line in Fig. 13(a)], we have a very good description of the  ${}^3S_1$  and  ${}^3D_1$  phase shifts, and we see that the mixing parameter has the

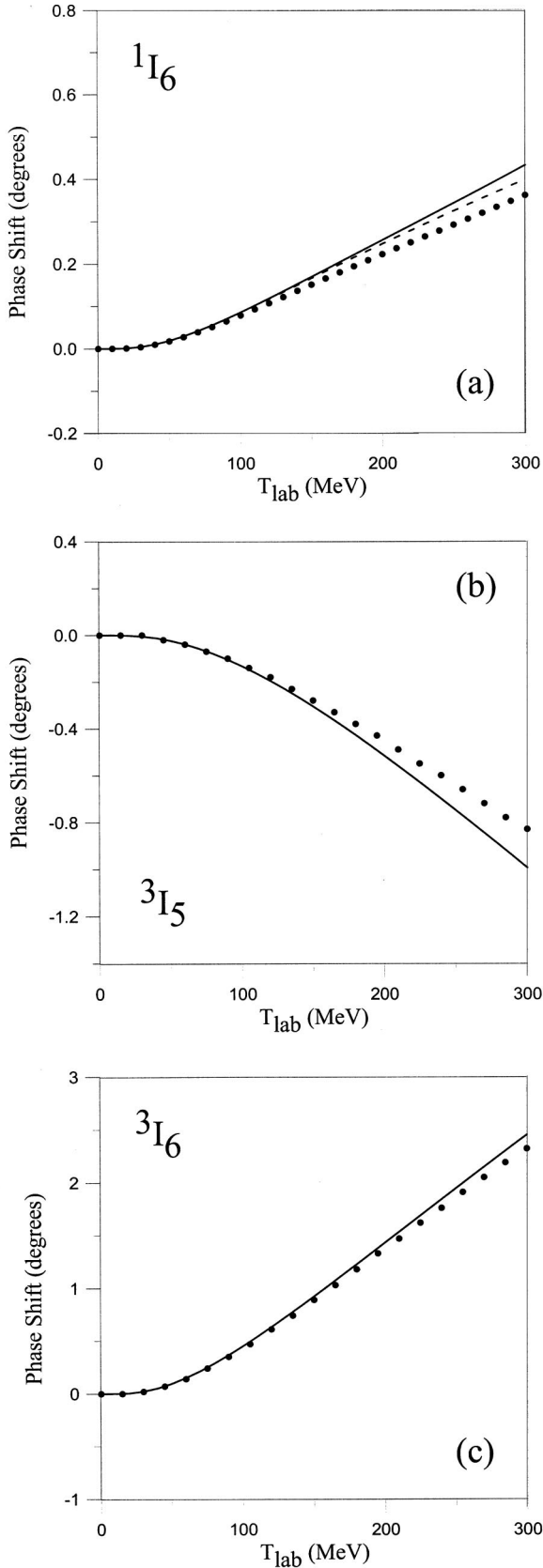


FIG. 11.  $NN$   $I$  phase shifts with  $J < 6$ . Lines have the same meanings as in Fig. 8.

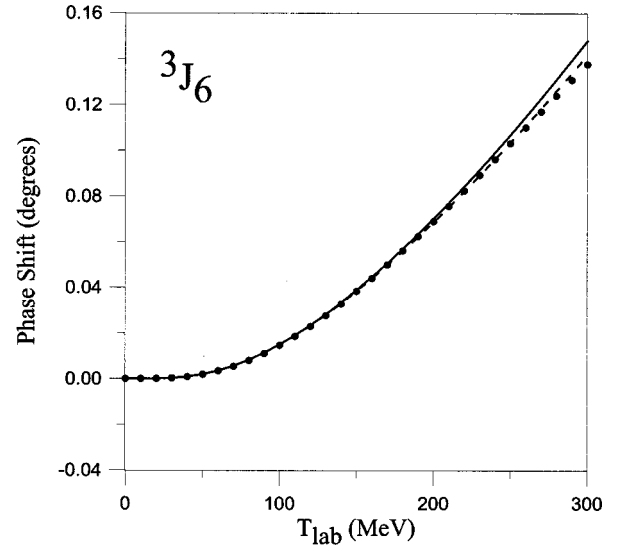


FIG. 12.  $NN$   ${}^3J_6$  phase shift. Lines have the same meanings as in Fig. 8.

right behavior only at very low energies. This seems to indicate the existence of a weak short-range tensor force, and the introduction of some new mechanism may be needed. If we include  $NN$  components only (dashed line), the result seems to be in better agreement with the experimental data. This is only due to the fact that the  ${}^3S_1$  phase shift has, in this case, a lower value and it is not an effect due to  $\Delta\Delta$  components.

Higher angular momentum mixing parameters are governed by the pseudoscalar tensor term and have a good agreement with the experimental data.

## VII. SUMMARY

Starting from the common belief that QCD is the underlying theory of the strong interaction, one is entitled to demand that hadron physics be formulated in terms of the basic quark degrees of freedom. Only in this way will we be able to describe the hadron structure and the hadron-hadron interaction in a consistent framework, and possibly shed some light on the true nature of nuclear forces. This work attempts to be a step in that direction. We use constituent quarks as the basic degrees of freedom in a model which incorporates a spontaneously broken symmetry of the QCD Lagrangian (the chiral symmetry). We are able to formulate QCD at low energy as an effective theory of massive quarks interacting through gluons and Goldstone bosons. Keeping the quark degrees of freedom (and not integrating them out, as done in effective field theories) is of capital importance in order to generate the short-range part of the  $NN$  interaction through the quark Pauli principle. As a consequence, one obtains a physical mechanism which does not resort to contact terms and limits the number of free parameters in the model. Besides, such a mechanism allows us to generate the short-range behavior of any other hadron-hadron potential in a completely parameter-free way.

For the solution of the two-body problem, we have developed a RGM calculation in momentum space. We have proposed a method to solve the resulting coupled-channel

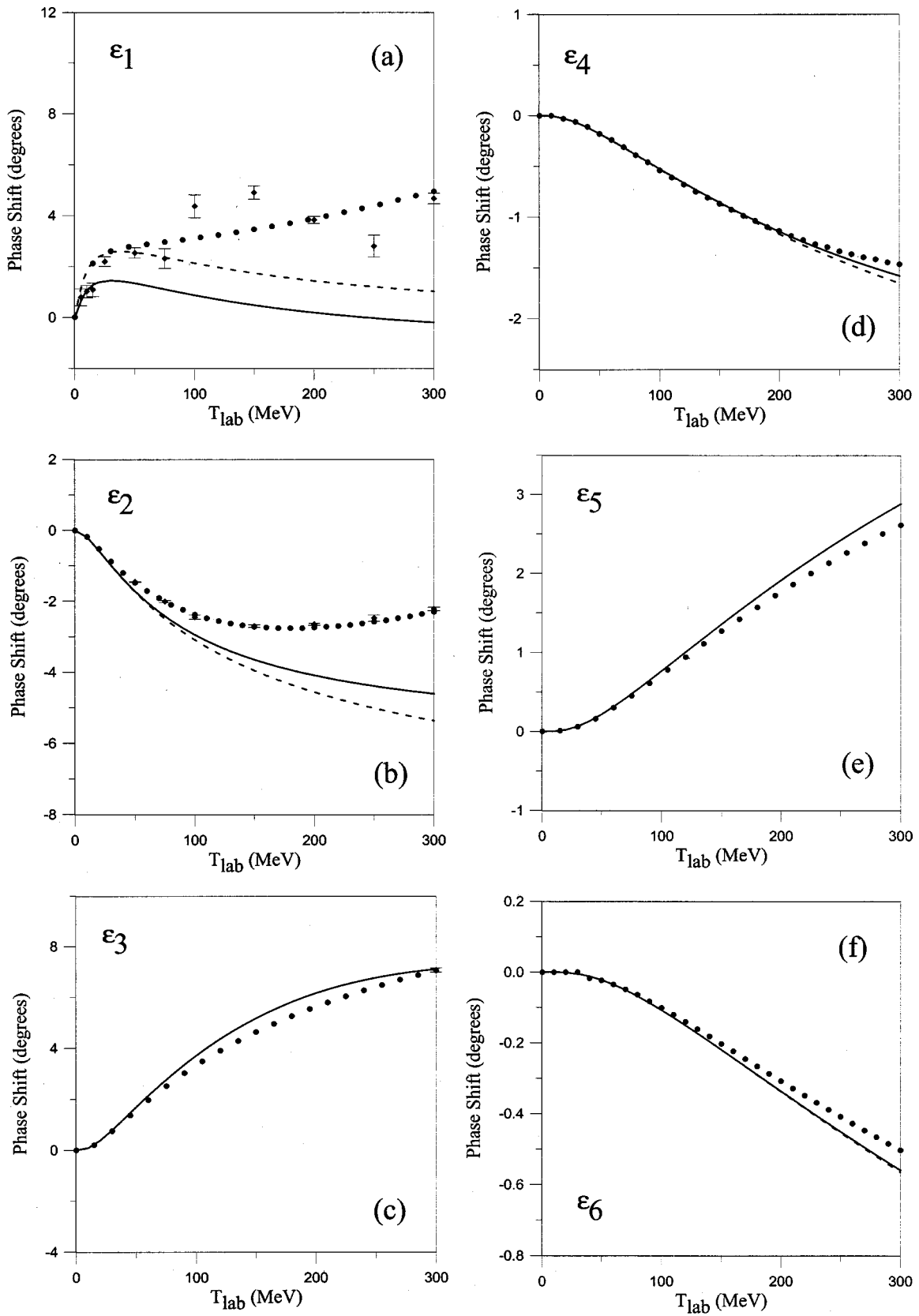


FIG. 13. Mixing parameter  $\epsilon$  for coupled  $NN$  partial waves. (a) Lines have the same meanings as in Fig. 3(b). All others labeled as in Fig. 8.

Lippmann-Schwinger equations. This new formalism will allow us to extend the calculation to above the pion threshold. Our method was used to obtain the  $NN$  scattering phase shifts (up to a total angular momentum  $J=6$ ), and the deuteron observables. Full couplings to  $N\Delta$  and  $\Delta\Delta$  channels were considered. The model here proposed is able to reproduce the  $NN$  phase shifts with good precision, except for the  ${}^3P_J$  waves. The  ${}^3P_J$  problem relates closely to the lack of a spin-orbit force in our potential, a topic which deserves special treatment outside this general work. Deuteron observables are also reproduced with high accuracy with the same model parameters.

For low angular momentum partial waves, the influence of the antisymmetry between quarks is very important, providing the short-range repulsion needed to reproduce the experimental data. The quark Pauli principle affects not only the  $S$  waves, but has also importance for the  $P$  waves.

The  $N\Delta$  components give an important contribution to the  ${}^1S_0^{NN}$  channel through the tensor coupling  ${}^1S_0^{NN} - {}^5D_0^{N\Delta}$ . This coupling, which plays a similar role to the  ${}^3S_1^{NN} - {}^3D_1^{NN}$  in the  ${}^3S_1^{NN}$  channel, provides the attraction needed to reproduce the experimental data. The coupling to  $\Delta\Delta$  channels can be quantitatively simulated by a slight modification of the model parameters. However, there are indications that certain observables (like the structure functions of the deuteron) require the presence of these components in the wave function of the deuteron. Higher angular momentum partial waves are dominated by the pseudoscalar interaction, and a good agreement with the experimental data is obtained.

The mixing parameters  $\epsilon_j$  deserve special mention. In general, they are well reproduced, except for  $\epsilon_1$  and  $\epsilon_2$ . While the disagreement for  $\epsilon_2$  can be easily understood, the case of  $\epsilon_1$  seems to indicate that there are details concerning the tensor force which are still missing in our model.

The present model, based on quite simple physical hypotheses and a reduced number of parameters, provides a promising description of the  $NN$  system below the pion threshold. The next step concerns the study above the pion threshold, which will be addressed in the near future.

#### ACKNOWLEDGMENTS

We thank Dr. A. Raspini for a careful reading of the manuscript. This work has been partially funded by Dirección General de Investigación Científica y Técnica (DGI-CYT) under Contract No. PB97-1410 and by Junta de Castilla y León under Contract No. SA-73/98.

#### APPENDIX

In this Appendix, we give the formulas needed for the calculation of the kernels appearing in Eq. (20). All results are written as operators in spin-isospin-color space. The corresponding matrix elements in these spaces are evaluated by means of standard SU(2) and SU(3) techniques [44].

The internal energy of each baryon appearing in Eq. (20) is calculated as

$$E_B = T_B^{int} + \langle B | V_{12}^{int} | B \rangle \quad (\text{A1})$$

TABLE VI. Coefficients for the RGM kernels of the Appendix.

$ij$	$a_{ij}$	$b_{ij}$	$c_{ij}$	$M_{ij}$
36	3/4	1/2	1/2	1
14	1	-1	1	4
13	11/16	-1/4	3/4	4
16	11/16	3/4	-1/4	4

with

$$T_B^{int} = \frac{3}{2m_q b^2},$$

$$V_{12}^{int} = 3 \times 4 \pi \int e^{-(b^2/2)q^2} V_{12}(q) q^2 dq. \quad (\text{A2})$$

The norm and kinetic energy exchange kernels appearing in Eq. (22) can be calculated analytically,

$$\begin{aligned} \text{RGM}_{N_E}(\vec{P}', \vec{P}_i) &= -9 \left[ \frac{3b^2}{4\pi} \right]^{3/2} \\ &\times e^{-(5/12)b^2(P'^2 + P_i^2) + (1/2)b^2 \vec{P}' \cdot \vec{P}_i} P_{36}^{STC}, \end{aligned} \quad (\text{A3})$$

$$\begin{aligned} \text{RGM}_{T_E}(\vec{P}', \vec{P}_i) &= \text{RGM}_{N_E}(\vec{P}', \vec{P}_i) \left\{ 3 \times \frac{3}{4m_q b^2} + \frac{1}{8m_q} \right. \\ &\left. \times (3P'^2 + 3P_i^2 - \vec{P}' \cdot \vec{P}_i) \right\}, \end{aligned} \quad (\text{A4})$$

where we use natural units ( $\hbar=c=1$ ) and  $P_{36}^{STC}$  is the exchange operator for quarks 3 and 6 in the spin-isospin-color space.

In general, the interactions kernels  $\text{RGM}_{V_D}(\vec{P}', \vec{P}_i)$  and  $\text{RGM}_{V_E}(\vec{P}', \vec{P}_i)$  for two-body potentials depending on momentum transfer are given by

$$V_{ij} = V_{ij}(\vec{p}'_{ij} - \vec{p}_{ij}) \delta^3(\vec{P}'_{ij} - \vec{P}_{ij}) \prod_{k \neq i,j} \delta^3(\vec{p}'_k - \vec{p}_k), \quad (\text{A5})$$

where  $V_{ij}(\vec{p}'_{ij} - \vec{p}_{ij})$  is the sum of the potentials with different spin-isospin-color dependences, and

$$\vec{p}_{ij} = \frac{1}{2}(\vec{p}_i - \vec{p}_j),$$

$$\vec{P}_{ij} = \vec{p}_i + \vec{p}_j. \quad (\text{A6})$$

The direct potential is given by

$$\text{RGM}_{V_D}(\vec{P}', \vec{P}_i) = 9 e^{-[b^2(\vec{P}' - \vec{P}_i)^2]^{1/3}} V_{qq}(\vec{P}' - \vec{P}_i), \quad (\text{A7})$$

while the exchange terms are

$$\begin{aligned} \text{RGM}V_{ijE}(\vec{P}', \vec{P}_i) &= -9M_{ij} \left[ \frac{3b^2}{4\pi} \right]^{3/2} \\ &\times e^{-b^2[(5/12)\vec{P}'^2 + (5/12)\vec{P}_i^2 - (1/2)\vec{P}' \cdot \vec{P}_i]} \\ &\times \int d\vec{q} e^{-b^2[a_{ij}\vec{q}^2 + b_{ij}\vec{q} \cdot \vec{P}' + c_{ij}\vec{q} \cdot \vec{P}_i]} \\ &\times V_{ij}(\vec{q})P_{36}^{STC}, \end{aligned}$$

$$\text{RGM}V_{12E}(\vec{P}', \vec{P}_i) = (V_{12}^{int} + V_{45}^{int}) \text{RGM}N_E(\vec{P}', \vec{P}_i), \quad (\text{A8})$$

where  $i$  and  $j$  refer to the pair of interacting quarks, and  $M_{ij}$  is a multiplicity factor indicating the number of equivalent interactions. The coefficients  $a_{ij}$ ,  $b_{ij}$ ,  $c_{ij}$ , and  $M_{ij}$  are given in Table VI.

Formulas (A7) and (A8) contain an angular integration which can be done explicitly for central and tensor-type potentials.

---

*Central potentials.*

$$\begin{aligned} \text{RGM}V_{ijE}(\vec{P}', \vec{P}_i) &= -9M_{ij} \left[ \frac{3b^2}{4\pi} \right]^{3/2} e^{-b^2[(5/12)P'^2 + (5/12)P_i^2 - (1/2)\vec{P}' \cdot \vec{P}_i]} 4\pi \\ &\times \int dq q^2 i_0(b^2q \sqrt{b_{ij}^2P'^2 + c_{ij}^2P_i^2 + 2b_{ij}c_{ij}\vec{P}' \cdot \vec{P}_i}) e^{-b^2a_{ij}q^2} V_{qq}(q) P_{36}^{STC}, \end{aligned} \quad (\text{A9})$$

where  $i_l(x)$  are the modified spherical Bessel functions of the first kind.

*Tensor potentials.* Assuming a tensor potential at quark level of the type

$$V_{ij}^T(\vec{q}) = V_c^T(q) [\vec{q} \otimes \vec{q}]^2 \cdot [\vec{\sigma}_i \otimes \vec{\sigma}_j]^2, \quad (\text{A10})$$

the result for the kernels is

$$\begin{aligned} \text{RGM}V_{ijE}^T(\vec{P}', \vec{P}_i) &= -9M_{ij} \left[ \frac{3b^2}{4\pi} \right]^{3/2} e^{-b^2[(5/12)P'^2 + (5/12)P_i^2 - (1/2)\vec{P}' \cdot \vec{P}_i]} 4\pi \int dq q^4 \frac{i_2(b^2q \sqrt{b_{ij}^2P'^2 + c_{ij}^2P_i^2 + 2b_{ij}c_{ij}\vec{P}' \cdot \vec{P}_i})}{b_{ij}^2P'^2 + c_{ij}^2P_i^2 + 2b_{ij}c_{ij}\vec{P}' \cdot \vec{P}_i} \\ &\times e^{-b^2a_{ij}q^2} V_c^T(q) [(b_{ij}\vec{P}' + c_{ij}\vec{P}_i) \otimes (b_{ij}\vec{P}' + c_{ij}\vec{P}_i)]^2 \cdot [\vec{\sigma}_i \otimes \vec{\sigma}_j]^2 P_{36}^{STC}. \end{aligned} \quad (\text{A11})$$

- 
- [1] R. Machleidt, *Adv. Nucl. Phys.* **19**, 189 (1989).
  - [2] S. Weinberg, *Nucl. Phys.* **B363**, 3 (1991).
  - [3] C. Ordóñez, L. Ray, and U. van Kolck, *Phys. Rev. C* **53**, 2086 (1996).
  - [4] E. Epelbaum, W. Glöckle, and Ulf-G. Meissner, *Nucl. Phys.* **A671**, 295 (2000).
  - [5] N. Kaiser, R. Brockmann, and W. Weise, *Nucl. Phys.* **A625**, 758 (1997).
  - [6] F. Fernández, A. Valcarce, U. Straub, and A. Faessler, *J. Phys. G* **19**, 2013 (1993).
  - [7] A. Faessler, F. Fernández, G. Lübeck, and K. Shimizu, *Phys. Lett.* **112B**, 201 (1982); *Nucl. Phys.* **A402**, 555 (1983).
  - [8] A. Valcarce, A. Faessler, and F. Fernández, *Phys. Lett. B* **345**, 367 (1995).
  - [9] E. V. Shuryak, *Phys. Rep.* **115**, 151 (1984).
  - [10] D. Diakonov and V. Petrov, *Nucl. Phys.* **B245**, 351 (1984).
  - [11] P. van Baal, *Nucl. Phys.* **B63**, 126 (1998).
  - [12] D. Diakonov, lectures at the Enrico Fermi School in Physics, Varenna, 1995 (unpublished).
  - [13] D. Diakonov, V. Petrov, and P. Pobylitsa, *Nucl. Phys.* **B306**, 809 (1988).
  - [14] A. Manohar and H. Georgi, *Nucl. Phys.* **B234**, 189 (1984).
  - [15] M. D. Scadron, *Yad. Fiz.* **56**, 245 (1993) [*Phys. At. Nucl.* **56**, 1595 (1993)].
  - [16] A. De Rújula, H. Georgi, and S. L. Glashow, *Phys. Rev. D* **12**, 147 (1975).
  - [17] K. Shimizu, *Rep. Prog. Phys.* **52**, 1 (1989).
  - [18] A. Valcarce, A. Buchmann, F. Fernández, and A. Faessler, *Phys. Rev. C* **51**, 1480 (1995).
  - [19] N. Isgur, *Phys. Rev. D* **62**, 014025 (2000).
  - [20] A. Valcarce, P. González, F. Fernández, and V. Vento, *Phys. Lett. B* **367**, 35 (1996).
  - [21] F. Fernández, A. Valcarce, P. González, and V. Vento, *Phys. Rev. C* **47**, 1807 (1993).
  - [22] Y. C. Tang, M. LeMere, and D. R. Thompson, *Phys. Rep.* **47**, 167 (1978).
  - [23] M. Kamimura, *Prog. Theor. Phys. Suppl. No.* **62**, 236 (1977).
  - [24] R. Machleidt, in *Computational Nuclear Physics 2: Nuclear Reactions*, edited by K. Langanke, J. A. Maruhn, and S. E. Koonin (Springer-Verlag, Berlin, 1993), pp. 1–29.
  - [25] H. P. Stapp, T. Ypsalantis, and N. Metropolis, *Phys. Rev.* **105**, 302 (1957).
  - [26] J. R. Bergervoet, P. C. van Campen, R. A. M. Klomp, J.-L. de Kok, T. A. Rijken, V. G. J. Stocks, and J. J. de Swart, *Phys. Rev. C* **41**, 1435 (1990).
  - [27] F. Fernández, A. Valcarce, P. González, and V. Vento, *Nucl. Phys.* **A567**, 741 (1994).
  - [28] V. A. Matveev and P. Sorba, *Lett. Nuovo Cimento Soc. Ital. Fis.* **20**, 435 (1977).

- [29] P. González and V. Vento, *Few-Body Syst.* **2**, 145 (1987).
- [30] E. Rost, *Nucl. Phys.* **A249**, 510 (1975).
- [31] L. Ya. Glozman and E. I. Kuchina, *Phys. Rev. C* **49**, 1149 (1994).
- [32] D. Allasia *et al.*, *Phys. Lett. B* **174**, 450 (1986).
- [33] H. Arenhövel, *Z. Phys. A* **275**, 189 (1975).
- [34] R. Dymarz and F. C. Khanna, *Nucl. Phys.* **A516**, 549 (1990).
- [35] M. Lacombe, B. Loiseau, J. M. Richard, R. Vinh Mau, J. Côté, P. Pirès, and R. de Tournreil, *Phys. Rev. C* **21**, 861 (1980).
- [36] J. Martorell, D. W. L. Sprung, and D. C. Zheng, *Phys. Rev. C* **51**, 1127 (1995); N. L. Rodning and L. D. Knutson, *Phys. Rev. Lett.* **57**, 2248 (1986); T. E. O. Ericson and M. Rosa-Clot, *Nucl. Phys.* **A405**, 497 (1983); C. van der Leun and C. Alderliesten, *ibid.* **A380**, 261 (1982).
- [37] W. P. Sitarski, P. G. Plunden, and E. L. Lomon, *Phys. Rev. C* **36**, 2479 (1987).
- [38] R. A. Arndt, C. H. Oh, I. I. Starkovski, R. L. Workman, and F. Dohrmann, *Phys. Rev. C* **56**, 3005 (1997).
- [39] SAID interactive program. Available on the Internet by telnet to *clsaid.phys.vt.edu* (mirror in *said-hh.desy.de*), user id: *said* or in the web site <http://clsaid.phys.vt.edu>.
- [40] D. R. Entem, F. Fernández, and A. Valcarce, *Phys. Lett. B* **463**, 153 (1999).
- [41] A. Valcarce, F. Fernández, and P. González, *Phys. Rev. C* **56**, 3026 (1997).
- [42] O. Dumbrajs, R. Koch, H. Pilkuhn, G. C. Oades, H. Behrens, J. J. de Swart, and P. Kroll, *Nucl. Phys.* **B216**, 277 (1983); T. L. Houk, *Phys. Rev. C* **3**, 1886 (1971); W. Dilg, *ibid.* **11**, 103 (1975); S. Klarsfeld, J. Martorell, and D. W. L. Sprung, *J. Phys. G* **10**, 165 (1984).
- [43] N. Kaiser, S. Gestendörfer, and W. Weise, *Nucl. Phys.* **A637**, 395 (1998).
- [44] D. R. Entem, Ph.D. thesis, University of Salamanca, 1999.